# Dynamics of Metastable Nanoscale Island Growth and Dissolution at Electrochemical Interfaces by Time-Resolved Scanning Tunneling Microscopy†

**Y. He and E. Borguet***

*Department of Chemistry and Surface Science Center, University of Pittsburgh, Pittsburgh, Pennsylvania 15260*

*Received: November 6, 2000; In Final Form: January 8, 2001*

The dynamics of nanoscale island growth, stability, and dissolution, accompanying the potential-induced phase transitions between the $(22 \times \sqrt{3})$ and $(1 \times 1)$ structures of the Au(111) surface in 0.1 M $HClO_4$ solution, have been investigated by potential pulse perturbation time-resolved scanning tunneling microscopy ($P^3$ TR-STM). Starting from a potential at which the reconstructed $(22 \times \sqrt{3})$ phase is stable, a short positive potential pulse briefly brings the electrode to a potential at which the $(1 \times 1)$ phase is stable. This pulse induces a perturbation that lifts the Au(111)−$(22 \times \sqrt{3})$ reconstruction completely, resulting in nanoscale island formation on the surface. The nanoscale islands are metastable and dissolve with time. The initial average island area and the island decay rate are related to the pulse amplitude and duration. The higher and longer the pulse, the smaller the average size of the islands produced and the more slowly the islands decay. This result reveals a "voltammetric annealing" process that may be important in stable island formation at electrochemical interfaces. The dynamics of individual islands are quite heterogeneous and nonmonotonic. Small islands decay faster than large islands. Even under metastable conditions, large islands frequently grow before ultimately decaying, providing evidence for electrochemical Ostwald ripening in this system. A simple model, based on perimeter detachment as the rate-limiting step, provides a qualitative explanation for the observed decay dynamics.

## 1. Introduction

The growth and stability of nanometer clusters on surfaces is of fundamental and technological importance. It is relevant to areas as diverse as epitaxy,[1,2] semiconductor interconnects, catalysis,[3] surface phase transitions,[4] and nanotechnology.[5] One of the principal challenges in the investigation of nanoscale growth and dissolution dynamics is the requirement of simultaneous temporal and spatial resolution of atomic and molecular processes on the relevant scales.[6] We have been pursuing this challenge with a particular focus on the electrochemical solid−liquid interface. Studying sequential scanning tunneling microscopy (STM) images enables relatively slow (>20 s) dynamics to be followed.[7] Faster changes can be investigated, in principle, by applying a voltage step perturbation during the acquisition of a given STM image: this is known as potentiodynamic STM.[8]

We have developed potential pulse perturbation time-resolved STM ($P^3$ TR-STM), an extension of potentiodynamic STM, to investigate the dynamics of metastable nanoscale $(1 \times 1)$ island growth, stability, and decay at the Au(111) interface. $P^3$ TR-STM (Figure 1) is the STM analogue of the pump−probe technique long used in optical studies. $P^3$ TR-STM involves applying a perturbation, here a short positive potential pulse, to the sample while the STM is imaging. This perturbation results in the creation of metastable state, i.e., a state that is not stable at the potential that exists after the perturbation. After the perturbing pulse, the evolution of the metastable state is followed in real time with STM. There is some controversy with regard to the definition of "time-resolved." While we do not capture an instantaneous image of the surface, the rate at which images are acquired is faster than most of the dynamics we observe. The 80 s it takes to acquire each image is shorter than the several hundreds of seconds it takes for the islands to dissolve.

The Au(111) surface provides an ideal system to study the dynamics of island growth and stability. The electrochemical environment provides a medium in which to control the dynamics. Au(111) has two stable phases: the unreconstructed $(1 \times 1)$ and the reconstructed $(22 \times \sqrt{3})$.[9] At room temperature, the $(22 \times \sqrt{3})$ phase is stable, while the first-order phase transition to the $(1 \times 1)$ phase requires heating to 880 K under ultrahigh vacuum (UHV).[10] In an electrochemical environment, however, the phase transition can be induced by changing the electrode potential. The existence of this phase transition in electrochemical environments was first suggested by classical voltammetry.[11] The relative roles of adsorption and surface charge in driving these phase transitions has been the object of debate.[12] Trace amounts of $Cl^-$ can enhance the mobility of gold atoms and reduce the stability range of the reconstructed structure.[13] Since the initial observation, the reconstruction has been confirmed by a number of techniques including second harmonic generation,[14−16] surface X-ray scattering,[17] and STM.[18−21] It is now well established that the reconstructed Au(111)−$(22 \times \sqrt{3})$ surface transforms to Au(111)−$(1 \times 1)$ phase at potentials above ~440 $mV_{SCE}$ and that the reverse transition occurs for potentials below ~220 $mV_{SCE}$ in $HClO_4$ solution.[19] The reconstructed $(22 \times \sqrt{3})$ surface is stable at potentials when the surface has a negative excess charge. The density of the reconstructed phase is estimated to be about 4.5% higher than the unreconstructed phase.[18] The dynamics of the phase transitions of Au(111) in electrolyte have been reported

† Part of the special issue "John T. Yates, Jr. Festschrift".
* To whom correspondence should be addressed.

10.1021/jp0040648 CCC: $20.00 
Published on Web 03/20/2001

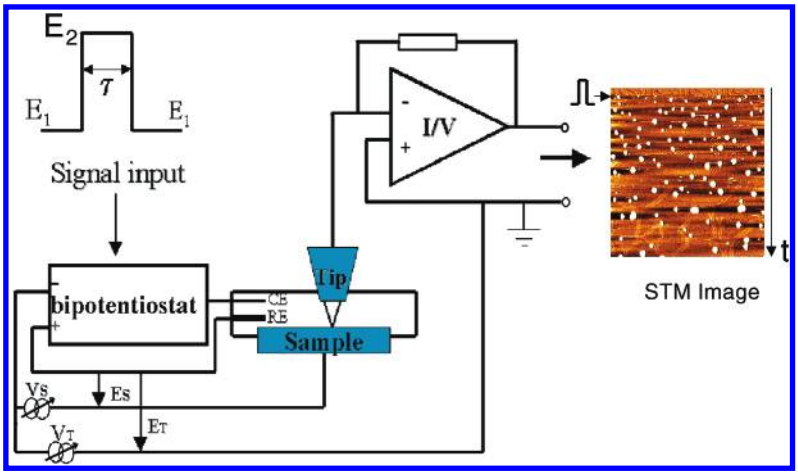


**Figure 1.** Schematic of potential pulse perturbation time-resolved STM ($P^3$ TR-STM). The perturbing pulse raises the sample potential from $E_1$ to $E_2$ for a time $\tau$ before returning the sample potential to the potential $E_1$. STM monitors the subsequent interfacial dynamics.

and shown to depend on the potential at which the transition occurs. However, there has been little focus on the growth and dissolution dynamics of the nanoclusters that are formed as a result. In particular, we show that quite distinct, but complementary, pictures emerge depending on whether one focuses on the overall island coverage, average island size, or the dynamics of individual islands. Our results show that the island decay rates are related to the pulse amplitude and duration. The higher and longer the pulse, the smaller the average size of the islands produced and the more slowly the islands decay. This result suggests a "voltammetric annealing" process that may be important in stable island formation. This phenomenon provides an explanation for the diverse kinetics reported previously for the phase transition.[9] Under metastable conditions, small islands decay while islands greater than a critical size, determined here to be 100 $nm^2$, frequently grow before ultimately decaying, providing evidence for electrochemical Ostwald ripening in this system.

## 2. Experimental Section

The Au(111) single crystal (Monocrystals Co.) was cleaned by immersion in hot piranha solution (1:3 $H_2O_2/H_2SO_4$) for 1 h and rinsed by ultrasonication in ultrapure water (18.2 MΩ) produced by a Barnstead Nanopure Infinity system. **(Caution! The piranha solution is a very strong oxidizing agent and extremely dangerous to handle in the laboratory. Protective equipment including gloves, goggles, and face shields should be used at all times.)** The crystal was hydrogen flame-annealed and allowed to cool to room temperature in air. The sample was transferred to the STM electrochemical cell and immersed under potential control (0.1 $V_{SCE}$) in 0.1 M $HClO_4$ solution. The sample was occasionally electropolished at 3 V potential in 1 M $H_2SO_4$ solution.[22] All electrode potentials are quoted in volts relative to the SCE potential ($V_{SCE}$).

STM images were obtained with a PicoScan STM system (Molecular Imaging Co.) with a bipotentiostat to control the sample and tip potential independently. The electrochemical cell was made of Teflon. A silver wire and a platinum wire were used as a quasi-reference electrode and counterelectrode, respectively. All cell components were chemically cleaned in the same way as the crystal. STM tips were prepared by electrochemically etching 0.25 mm diameter tungsten wires with 10 V AC, in 3 M KOH solution. Tips were coated with paraffin wax, yielding less than 10 pA of Faradaic current. All the STM images were obtained under constant current mode at ≈1 nA, 0.05 V tip−sample bias**.** All the images are presented unfiltered. The single island area and island coverage were measured by Visual-SPM software (Molecular Imaging).

The STM experimental setup does not restrict access of the electrolyte to the interface as it would in a thin cell optical configuration. All our experiments, even with pulses as short as 0.1 s, indicate a very rapid lifting of the reconstruction, suggesting a time constant significantly less than 1 s. Furthermore, because of the rastering nature of the STM experiment, no significant portion of the surface is under the tip for more than a fraction of a second.

No evidence for tip-assisted dynamics was observed. There was no evidence of mechanical contact with the surface. The sample region (a segment a few nanometers by 296 nm) over which the electrode potential was pulsed did not show any pits or other features that distinguished it from the rest of the surface. In several instances we have zoomed out to explore a larger area and saw no apparent differences between the smaller repeatedly scanned area and the larger area that surrounded it.

The $P^3$ TR-STM experiment is illustrated schematically in Figure 1. The sample was initially held, in all the experiments reported here, at a potential (0.1 $V_{SCE}$) at which the reconstructed ($22 \times \sqrt{3}$) structure is stable. A short positive potential pulse was applied to the sample while the STM was imaging. This results in the rapid lifting of the surface reconstruction. After the perturbing pulse, the sample returns to its initial potential. The STM follows the dynamics on a frame-by-frame basis. The scan direction is indicated by an arrow at the right of each image and also serves as a time axis. Improved time resolution can be obtained by dividing an image into multiple horizontal slices. This approach is valid as long as the slice is large enough to be representative of the overall surface. A series of experiments, involving perturbing pulses of 0.8 and 0.9 $V_{SCE}$ amplitude and 0.1, 0.2, 0.5, 1, 2, 5, and 10 s duration was performed.

## 3. Results and Discussion

The characteristic herringbone pattern of the reconstructed surface, with stripes separated by 6.3 nm, is clearly seem in the STM image presented in Figure 2A. This is in agreement with previous observations.[19,20] Domains oriented at 120° to each other are clearly observed. Figure 2B shows the surface after a 2 s, 0.9 $V_{SCE}$ pulse, is applied. When the potential is increased rapidly to a high value, the reconstruction is immediately lifted to yield the less dense ($1 \times 1$) phase. The lifting of the reconstruction appears to be complete as the characteristic herringbone pattern of reconstructed stripes disappears entirely,

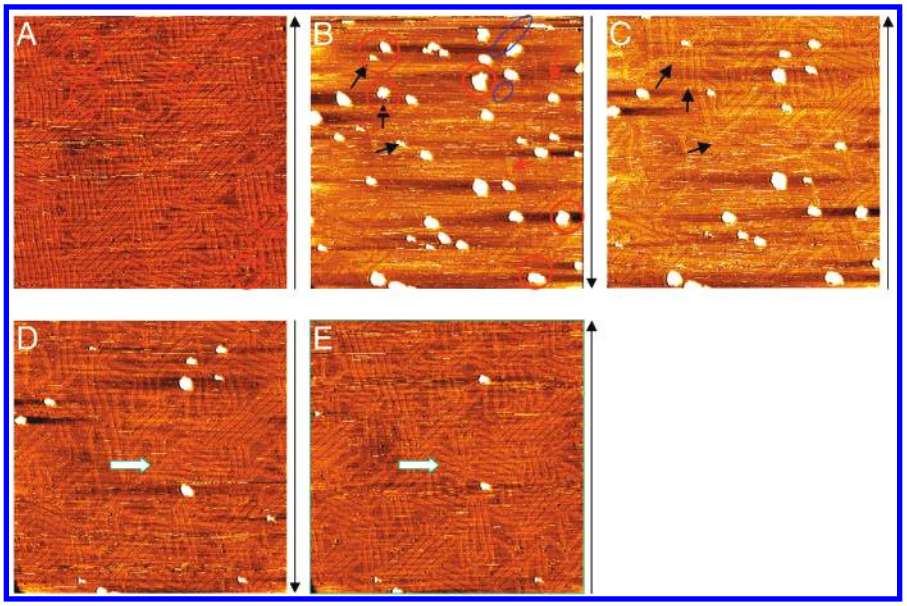


**Figure 2.** (A) STM image (296 nm × 296 nm) of Au(111)/0.1M $HClO_4$ at 0.1 V (vertical scale 1.5 Å). Reconstruction is clearly indicated by 6.3 nm wide stripes oriented in domains at 120° to each other. The images were acquired at 512 × 512 resolution, at a rate of 6 lines/second resulting in one image approximately every 85 s. Red circles indicate domain boundaries or defects where islands subsequently appear. (B) STM image (296 nm × 296 nm) of Au(111)/0.1M $HClO_4$ at 0.1 V, 0−80 s after a 2 s, 0.9 V pulse (vertical scale 1.5 Å). Islands result from the lifting of the reconstruction. Red circles indicate some of the islands that have appeared at domain boundaries or defects identified in panel A. Islands appear at sites that in panel A were associated with domain boundaries or defects. These can be considered as nucleation sites for either the lifting of the reconstruction or the growth of Au(111)−(1 × 1) islands. Blue ellipses indicate faint reconstruction stripes. Red arrows point to reconstructed stripes whose direction is different from stripes in the same region in panel A. (C) Au(111)/0.1M $HClO_4$ at 0.1 V, 81−165 s after a 2 s, 0.9 V pulse (vertical scale 1.5 Å). (D) Au(111)/0.1 M $HClO_4$ at 0.1 V, 166−250 s after a 2 s, 0.9 V pulse (vertical scale 1.5 Å). (E) Au(111)/0.1 M $HClO_4$ at 0.1 V, 251−335 s after a 2 s, 0.9 V pulse (vertical scale 1.5 Å).

and islands appear. The extra Au atoms of the reconstructed $(22 \times \sqrt{3})$ phase are ejected onto the surface. Some fraction of the excess atoms renucleate into reconstructed stripes that are thermodynamically favored at the post-pulse potential (0.1 $V_{SCE}$). Some fraction of these excess atoms are mobile and nucleate into monolayer high clusters.[19] The growth of the (1 × 1) islands presumably occurs in the following steps. First, nucleation sites are formed at the intersection of reconstructed domains. This is indicated by the high degree of correlation between the position of islands in Figure 2B and domain intersections or voids in Figure 2A, highlighted by the red circles in both figures. Second, mobile surface Au atoms diffuse and attach at these nucleation sites leading to island growth.

As time increases, i.e., as the scan proceeds down the image, the single island area increases but the density of islands decreases. Simultaneously the area covered by reconstruction stripes increases. The upper half of the Figure 2B contains 26 islands of average size 54.6 $nm^2$. The lower half of the image contains 18 islands of average size 65.8 $nm^2$. This indicates that some clusters dissolve, while other clusters grow larger. Atoms released by dissolving clusters can attach to remaining islands, accounting for the increased average island size in the lower half of the image. Released atoms can also contribute to the regrowth of the reconstructed phase, as indicated by the greater density of reconstruction stripes in the lower half. Some islands that disappear by the succeeding image, Figure 2C, are indicated by arrows. The dissolution of clusters supplies atoms to form larger clusters that appear stable at the negative potential that now characterizes the surface, as well as to form the reconstructed $(22 \times \sqrt{3})$ phase.

At the top of Figure 2B a few, isolated reconstructed stripes are present. They represent a small fraction of the total area, indicating that >95% of the reconstruction was lifted. In addition, it is clear that the direction of some of the reconstructed stripes, indicated by red arrows in Figure 2B, is different from stripes at the same location in Figure 2A, suggesting that these stripes are new. As time elapses further, the area covered by reconstructed domains increases. Smaller islands continue to act as nucleation points for the new reconstructed domains. The evaporation of the small islands appears to provide the Au atoms that constitute the reconstructed stripes. It should be noted that the reconstructed phase is still fluxional. In particular, the reconstructed stripes can change direction and size until stable domains form, as illustrated by inspection of areas indicated by the open arrows in Figure 2D,E. In each case the direction of the reconstructed stripes changes from panel D to panel E.

**3.1. Overall Island Dissolution Dynamics.** The overall dissolution dynamics of the nanoclusters can be studied by plotting the fractional island coverage, i.e., fraction of the surface covered by islands, as a function of time. Figure 3 shows the time dependence of the fractional island coverage after 0.8 and 0.9 $V_{SCE}$ potential pulses of 1, 2, 5, and 10 s duration. The indicated time is the average time for the image or slice, after the application of the perturbation. The extrapolation back to zero time, indicated by the dotted line, suggests that the initial fractional island coverage is lower than the 4.5% reported in the literature.[18] Furthermore, the lower the pulse potential and the shorter the pulse duration, the lower the initial coverage. Possible reasons for the lower apparent initial island coverage may be as follows: (1) the lower potential and short duration pulse did not lift the reconstruction completely; (2) not all ejected atoms form islands and instead remain as mobile atoms; (3) mobile atoms are incorporated into steps.

While all these mechanisms probably contribute to the observed dynamics, we argue that scenario 2 dominates. Our data suggest that the first mechanism makes but a small contribution. Experiments have been performed with pulses ranging from 0.1 to 10 s in duration. In all cases we see an almost complete removal of the reconstruction stripes in the area scanned immediately after the pulse. Clearly, because after

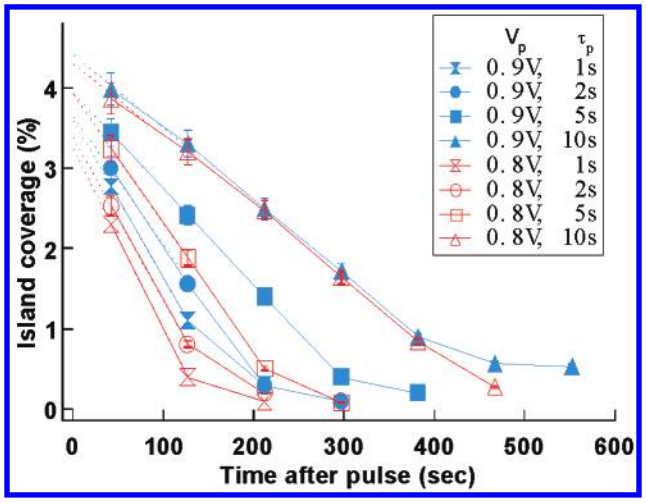


**Figure 3.** Fractional Au(111)−(1 × 1) island coverage as a function of time after the perturbing potential pulse. The dotted lines represent linear extrapolations back to zero time as discussed in the text.

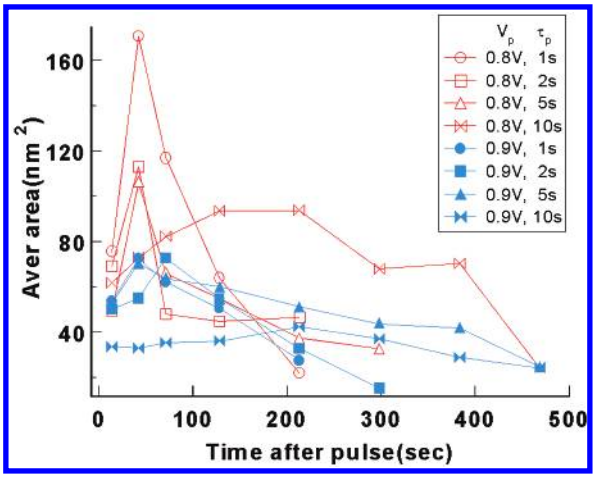


**Figure 4.** Average island area, the total area covered by islands divided by the number of islands, for different perturbing pulse amplitudes and duration.

the pulse the sample is at a potential at which the reconstructed phase is stable, some reconstruction stripes will appear. The stripe direction is determined by the underlying lattice. There are three principal directions for the (111) lattice. Hence, there is a 33% probability that a new stripe will be in the same direction. If all the stripes are in the same direction as before the pulse, then one can conclude that the reconstruction was not lifted. However, of the already small number of reconstructed stripes in Figure 2B only about 50% have the original direction. It appears reasonable to conclude that the reconstruction was almost completely lifted by the perturbing pulse. In addition, incorporation of mobile atoms into steps would be favored by longer pulses, which would allow the atoms more time to reach the distant steps than short pulses.[19] It has been reported that atom self-diffusion depends strongly on potential and adatom diffusion is effectively quenched at about 0.0 $V_{SCE}$.[23] Assuming a random walk on a the surface ($D = L^2/2t$), the distance traveled ($L$) in 1 s ($t$) ranges from 0.4 to 14 nm for values of the diffusion constant, $D$, ranging from $10^{-15}$ cm$^2$ s$^{-1}$. at 0.0 $V_{SEC}$ to $10^{-12}$ cm$^2$ s$^{-1}$ at 0.9 $V_{SEC}$. This is shorter than the distance between steps on our surface (>200 nm). Consequently, it would appear that short pulses do not enable mobile atoms to effectively attach to the growing nucleation sites, hence the lower apparent initial coverage. The nucleation sites and islands that result from shorter pulses appear to be less attractive "traps".

Four points deserve to be noticed:

(1) The fraction of the surface covered with islands decays linearly with time until low coverage, i.e., less than 0.5%. The linear rate of decay suggests that the decay rate is independent of island area. Rather it depends on the properties of the initial state of the island and/or the surface.

(2) The rate at which the fractional island coverage decreases depends strongly on the perturbing pulse potential and duration. The longer the pulse and the greater its amplitude, the slower the islands dissolve. This suggests that the island decay rate depends not only on the sample potential, as observed by Tao et al.,[19] but also on the pulse potential and duration that led to the formation of the islands in the first place. This behavior is different from that reported earlier, in which the surface self-diffusion of Au atoms at constant temperature in acid solution was found to depend only on the electrode potential.[23,24] Our observation suggests that atom diffusion is not the rate-limiting step in either island growth or dissolution. More likely atom detachment from the island perimeter is now the rate-limiting step. This conclusion is supported qualitatively by a simple model we use to explain the dynamics of single islands in a later section. These conclusions also apply to the dynamics of the reconstruction that depend on the disappearance of the islands.

(3) For perturbing pulses of 10 s duration, the islands formed by 0.8 and 0.9 V pulses decay at almost the same rate. This suggests that the 10 s pulse duration results in the formation of stable nanoscale islands. We deduce that the long pulse duration at higher potential makes the islands more stable and that 10 s may be a characteristic time for stable island formation. This suggests a "voltammetric annealing" process, analogous to the structural stability induced by metallurgical annealing at high temperature. It is distinct from "electrochemical annealing" that, on the contrary, results in the disappearance of islands due to anion-enhanced mobility.[25] The concept of "voltammetric annealing" may offer an explanation for the observed decrease transition rate from Au(100)−(1 × 1) to Au(100)−(hex) with the length of time at which the Au(100)−(1 × 1) surface was held at positive potentials.[26] Holding the surface at a positive potential results in "voltammetric annealing" of the island structures that characterize the Au(100)−(1 × 1) phase and that are one of the major sources of atoms needed to make the higher density Au(100)−(hex) reconstructed phase. Unfortunately we were not able to obtain atomic resolution images of the islands to further probe their structure and possible presence of defects within them that could be annealed out by longer pulses.

(4) The nanoisland dissolution dynamics slow for all perturbing pulses, as the fractional island coverage approaches zero. The last remaining islands seem to disappear with great difficulty, indicating an enhanced stability.

**3.2. Evolution of Average Island Area vs Time.** The evolution of the average island area, defined as the total area covered by islands divided by the number of islands, is shown in Figure 4 for perturbing pulse amplitudes of 0.8 and 0.9 V and pulse durations from 1 to 10 s. Improved time resolution, for the initial dynamics after the pulse perturbation, is obtained by dividing the first image into three horizontal stripes and associating a time with each stripe. In this way the overall dynamics, though not individual island dynamics, can be investigated. The average island area, immediately after the perturbing pulse, depends on the pulse potential and pulse duration. The *higher* the pulse potential and the *longer* the pulse duration, the *smaller* the initial average island area. Thus while

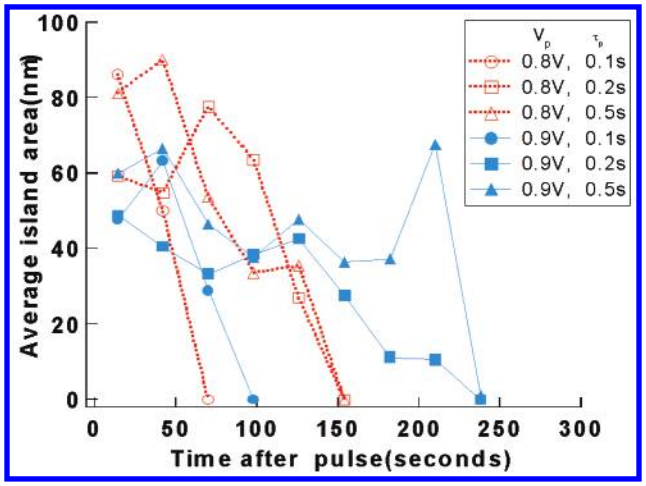


**Figure 5.** Average island area, the total area covered by islands divided by the number of islands, for short perturbing pulse duration (<1 s).

long, high pulses create more stable islands, i.e., islands that decay more slowly, they are also smaller. This would appear to suggest that smaller islands are more stable. However, investigation of individual island dynamics, discussed below, show this not to be the case.

Contrary to the fractional island coverage, the average island area does not initially decrease with time after the potential pulse perturbation. In fact, the average island area typically increases before decreasing. The time scale over which the initial increase occurs depends on the perturbing pulse. The rate of increase also shows a correlation with the nature of the perturbation: the longer the pulse, the slower the increase. For short pulses, the increase in average island size only becomes apparent by examining the dynamics at early times. The horizontal time slice approach, which yields the initial three data points, for $t < 100$ s, in Figure 4, enables the fast initial rise to be resolved for the short pulses. The growth and dissolution phases are much slower for the 10 s pulses and can be resolved directly, without resort to the horizontal time slice approach. This is consistent with the result in section 3.1 that the 10 s pulse duration results in the formation of stable nanoscale islands.

The dissolution kinetics associated with shorter pulses (<1 s) were too rapid to be observed on a frame-by-frame basis in our experiments. However, using the complementary approach of dividing an image into several horizontal stripes and associating a time with each stripe, the overall dynamics are shown in Figure 5. The fluctuations observed in the data are a consequence of the statistics of small numbers of islands in our slices, an area equal to a third of a frame. However, the following qualitative observations can be made. For the very shortest pulses, 0.1 s, a rapid decay of average island area is observed. The longer and greater the pulse, the slower the average island area decays. Clearly, 0.9 V pulses of 0.2 and 0.5 s duration result in nanoscale island distributions that maintain their average island area longer than 0.8 V pulses of the same duration. The results shown in Figure 5 are therefore consistent with the notion of "voltammetric annealing": longer and higher pulses result in more stable island populations.

Improved time resolution clearly has much to offer. On the basis of frame-by-frame analysis it appeared that only in some cases, such as after 0.8 V (10 s) and 0.9 V (10 s) pulse perturbation, did the average island area increase first and decrease later. In the case of low-voltage, short-duration pulse perturbations, island growth was rarely observed. After such short perturbations, the island decay rate is so fast, and the process completes within such a short time, that the initial growth phase cannot be observed with frame-by-frame time resolution. The rapid island decay rate obscures any growth. However, on the basis of horizontal time slice analysis, which supplies the extra data points, the initial growth phase is observed for the shorter pulses, i.e., less than 10 s. While island growth and decay are simultaneous and competing processes, the initial conditions play a large role in determining their relative importance.

The observation that high pulse potential and long pulse duration result in islands with small average area, and low pulse potential and short pulse duration result in islands with large average area, can also be explained. Upon applying the pulse potential perturbation, all the extra Au atoms from the Au(111)$-(22 \times \sqrt{3})$ phase are ejected onto surface. These mobile atoms diffuse to nucleation sites, where they attach to form small islands. Our observations suggest that the stability of these islands depends on the pulse potential and pulse duration. The high pulse potential and long pulse duration result in stable islands, whereas for the low pulse potential and short duration these islands are not stable. When the potential returns to the initial value at which the reconstructed structure is stable, the phase transition from Au(111)$-(1 \times 1)$ to Au(111)$-(22 \times \sqrt{3})$ occurs, and the islands begin to decay. The stable islands formed in the case of high potential and longer duration pulse decay more slowly, so that many small islands, as well as the larger islands, are observed. The islands formed in the case of lower potential and short duration pulse, on the other hand, are not as stable. They decay faster, with small islands disappearing first. With our current time resolution we see a lower initial density (Figure 3), dominated by larger islands. Hence it appears that a larger average island area is associated with smaller lower pulses (Figure 4). These distributions have been depleted of smaller islands, raising the average island area.

It is clear that the evolution is nonmonotonic and that the island populations are inhomogeneous in their dynamics. While the islands are in a metastable state after the pulse, some islands continue to grow while others disappear rapidly. To understand the process of island decay more clearly, we need to investigate the dynamics of individual islands.

**3.3. Individual Island Dissolution Dynamics.** Inspection of the STM images in Figure 2 indicates that the island size is inhomogeneous. The data shown in Figures 2, 4, and 5 also suggest that the island dynamics are neither homogeneous nor monotonic. By following the evolution of individual islands, some slow decay processes were found for islands formed after 0.8 V (10 s), 0.9 V (5 s), and 0.9 V (10 s) pulses. In these experiments the smaller islands decay first and disappear rapidly. However, big islands grow before they decay. The growth of the large islands persists longer than 100 s following an 0.8 V, 10 s pulse (Figure 6). The "initial area" of those islands is greater than 100 nm$^2$. The growth of large islands at the apparent expense of smaller islands is termed Ostwald ripening.[27] The linear rate of decay suggests that the decay rate is independent of island area. If the decay did depend on area, one would expect the slope to change as the islands become smaller. Rather, the rate of decay appears to depend on other properties of the initial island, such as its initial size.

A simple model, based on detachment of atoms from the island perimeter as the rate-limiting step, provides qualitative agreement with the data and insight into the evaporation dynamics. Let $A_0$ be the initial island area, $A$ the area at any time $t$, and $k$ the rate of detachment from the island perimeter. The island evaporation rate can be written as

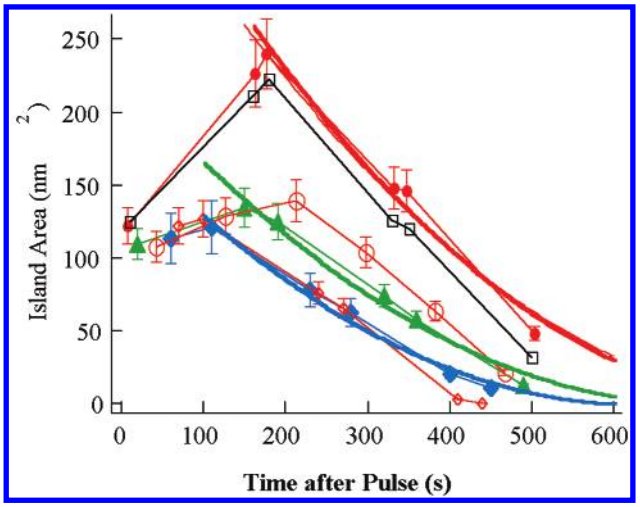


**Figure 6.** Dynamics of six individual long-lived islands formed after a 10 s, 0.8 V pulse. The thick solid lines are representative fits, for the data represented by solid symbols, to the perimeter atom detachment model described in the text, for three islands. The other islands show similar behavior.

$$dA/dt = -k(A)^{0.5} \quad (1)$$

and the island area, $A$, determined by integration of eq 1 as

$$A = A_0 - [k(A_0)^{0.5} - k^2t/4]t \quad (2)$$

This model, the results of which are shown for three islands in Figure 6, qualitatively reproduces the decay of the islands. At short times, i.e., $t \ll 4k(A_0)^{0.5}$, the rate is determined by the initial island size. This explains why the rate also appears independent of island size at early times, as observed above. Furthermore, the model qualitatively reproduces the quasi-linear dependence of the island dissolution rate at early times, i.e., $A(t) = A_0 - k(A_0)^{0.5}t$. At long times the term in $k^2t^2/4$ becomes important and results in a leveling off of the decay rate, consistent with our experimental observations. Similar values ($0.045 \pm 0.005$ nm/s) of the rate constant, $k$, are determined for the islands analyzed in Figure 6. This rate corresponds to the detachment of about 1 atom every 6 s from the perimeter of an island.

The observed linear time dependence of the decay rate is similar to literature reports of small Au island decay on Au (111) and Au(100) single crystals in $H_2SO_4$ solution.[24] Similar kinetics are reported for the disappearance of metastable ($7 \times 7$) domains on Si(111),[4] and the decay of STM induced silicon islands and craters.[28] In addition, the island decay dynamics appear to show a strong inverse correlation with maximum size achieved before decay begins. A similar, strong inverse correlation of the island decay rates with the initial size was observed on Si(111).[4] The dynamics of ($7 \times 7$) islands on Si(111) show no evidence of Ostwald ripening, whereas the nanoscale Au islands observed here do. It would appear that a more detailed analysis is required to draw more extensive conclusions.

## 4. Conclusion

Potential pulse perturbation time-resolved scanning tunneling microscopy ($P^3$ TR-STM) has been used to investigate the growth and dissolution dynamics of nanoscale islands. The island dynamics are heterogeneous and nonmonotonic. The properties (size, distribution, lifetime, ...) of the islands can be controlled by tailoring the potential pulse perturbation. The average island area depends on the amplitude and duration of the perturbing pulse that leads to their formation. The higher and longer the pulse, the smaller the islands. The island dissolution rate depends on pulse potential and duration. The higher the potential and the longer the pulse, the slower the decay rate. Small islands decay first, providing the mobile Au atoms and the nucleation sites for the formation of the reconstructed ($22 \times \sqrt{3}$) structures. Small islands also decay more rapidly than large islands, leading to an increase in the average island size. A subset of the population, typically islands greater than 100 nm$^2$, grow first and decay at longer times. A simple model based on perimeter atom detachment qualitatively reproduces the observed behavior. These results offer new insight into the growth and decay of nanoscale objects at interfaces and elucidate the dynamics of the phase transition itself. $P^3$ TR-STM offers a novel means to investigate the dynamics of metastable nanostructures at interfaces in real time.

**Acknowledgment.** We acknowledge the generous support of the NSF. E.B. acknowledges the NSF for a CAREER award (CHE-9734273) and the Research Corporation for a Research Innovations Award in support of this research. We thank Professor David Waldeck for a critical reading of the manuscript and useful suggestions. Pertinent comments and suggestions by the reviewers are acknowledged.

## References and Notes

(1) Villegas, I.; Napolitano, P. *J. Electrochem. Soc.* **1999**, *146*, 117.
(2) Giesen, M.; Icking-Konert, G. S.; Ibach, H. *Phys. Rev. Lett.* **1998**, *80*, 552.
(3) Valden, M.; Lai, X.; Goodman, D. W. *Science* **1998**, *281*, 1647.
(4) Hannon, J. B.; Hibino, H.; Bartelt, N. C.; Swartzentruber, B. S.; Ogino, T.; Kellogg, G. L. *Nature* **2000**, *405*, 552.
(5) Kolb, D. M.; Ullmann, R.; Will, T. *Science (Washington, DC)* **1997**, *275*, 1097.
(6) Kolb, D. M. *Electrochim. Acta* **2000**, *45*, 2387.
(7) Gao, X. P.; Weaver, M. J. *Ber. Bunsen-Ges. Phys. Chem. Chem. Phys.* **1993**, *97*, 507.
(8) Gao, X. P.; Edens, G. J.; Hamelin, A.; Weaver, M. J. *Surf. Sci.* **1993**, *296*, 333.
(9) Kolb, D. M. *Prog. Surf. Sci.* **1996**, *51*, 109.
(10) Huang, K. G.; Gibbs, D.; Zehner, D. M.; Sandy, A. R.; Mochrie, S. G. J. *Phys. Rev. Lett.* **1990**, *26*, 3313.
(11) Kolb, D. M.; Schneider, J. *Electrochim. Acta* **1986**, *31*, 929.
(12) Wu, S.; Lipkowski, J.; Magnussen, O. M.; Ocko, B. M.; Wandlowski, T. *J.Electroanal. Chem.* **1998**, *446*, 67.
(13) D'Agostino, A. T.; Ross, P. N. *Surf. Sci.* **1987**, *185*, 88.
(14) Friedrich, A.; Pettinger, B.; Kolb, D. M.; Luepke, G.; Steinhoff, R.; Marowsky, G. *Chem. Phys. Lett.* **1989**, *163*, 123.
(15) Luepke, G.; Marowsky, G.; Steinhoff, R. *Phys. Rev. B: Condens. Matter* **1990**, *41*, 6913.
(16) Friedrich, A.; Shannon, C.; Pettinger, B. *Surf. Sci.* **1991**, *251−252*, 587.
(17) Wang, J.; Ocko, B. M.; Davenport, A. J.; Isaacs, H. S *Phys. Rev. B: Condens. Matter* **1992**, *46*, 10321.
(18) Gao, X.; Hamelin, A.; Weaver, M. J. *J. Chem. Phys.* **1991**, *95*, 6993.
(19) Tao, N. J.; Lindsay, S. M. *Surf. Sci. Lett.* **1992**, *274*, L546.
(20) Tao, N. J.; Lindsay, S. M. *J. Appl. Phys.* **1992**, *70*, 5141.
(21) Kolb, D. M.; Dakkouri, A. S.; Batina, N. In *Nanoscale Probes of the Solid/Liquid Interface*; Gewirth, A. A., Siengenthaler, H., Eds.; Kluwer: Dordrecht, The Netherlands, 1995; NATO ASI Vol. E288, p 263.
(22) Whitton, J. L.; Davies, J. A. *J. Electrochem. Soc.* **1964**, *111*, 1347.
(23) Hirai, N.; Nishide, M.; Hara, S. *Surf. Sci.* **1995**, *340*, L965.
(24) Hirai, N.; Watanable, K. I.; Shiraki, A.; Hara, S. *J. Vac. Sci. Technol. B* **2000**, *18*, 7.
(25) Treavor, D. J.; Chidsey, C. E. D.; Loiacono, D. N. *Phys. Rev. Lett.* **1989**, *62*, 929.
(26) Schneider, J.; Kolb, D. M. *Surf. Sci.* **1988**, *193*, 579.
(27) Stabel, A.; Heinz, R.; Deschryver, F. C.; Rabe, J. P. *J. Phys. Chem.* **1995**, *99*, 505.
(28) Tanaka, Y.; Ishiyama, K.; Ichimiya, A. *Surf. Sci.* **1996**, *357−358*, 840.